

HOT DEFORMATION BEHAVIOR OF A N-BEARING AUSTENITIC STAINLESS STEEL BIOMATERIAL¹

*Eden Santos Silva²
Regina Célia de Sousa³
Alberto Moreira Jorge Junior²
Oscar Balancin²*

Abstract

An austenitic stainless steel (ISO 5832-9) with an intermediate level of stacking fault energy (SFE) was torsion-deformed at temperatures ranging from 900°C to 1,200°C and at strain rates ranging from 0.01 s⁻¹ to 10 s⁻¹. The hot deformation behavior was analyzed based on variations in the shape of flow stress curves, a constitutive equation, processing maps and the final microstructures. A region of instability in the temperature-strain rate space was observed at low temperature and high strain rates, and domains of easy processing were determined at high and intermediate temperatures and low strain rates. The final microstructure was analyzed based on the evolution of the internal structure over time in response to hardening and softening mechanisms such as work hardening, recovery and recrystallization.

Key words: Biomaterial; Stainless steel; Workability; Processing map.

DEFORMAÇÃO A QUENTE DO AÇO INOXIDÁVEL AUSTENITICO ALTO NITROGÊNIO UTILIZADO COMO BIOMATERIAL

Resumo

Um aço inoxidável austenítico (ISO 5832-9) com energia de falha de empilhamento (EFE) intermediária foi deformado por torção a quente num intervalo de temperatura de 900°C – 1.200°C e taxa de deformação entre 0,01 s⁻¹- 10 s⁻¹. O comportamento da deformação foi analisada baseado na variação na forma das curvas de escoamento plástico, equações constitutivas, mapas de processamento e análise microestrutural. A região de instabilidade no espaço temperatura - taxa de deformação, foi analisado na região de baixa temperatura e alta taxa de deformação, os dominios de boa processabilidade foi determinado na região de temperatura intermediária e baixa taxa de deformação. A microestrutura final foi analisada baseada na evolução da estrutura interna em resposta ao mecanimos de enduecimento e amaciamento dinâmico, tais como encruamento, recuperação e recristalização dinâmica.

Palavras-chave: Biomaterial; Aço inoxidável; Trabalhabilidade; Mapas de processamento.

¹ *Technical contribution to 67th ABM International Congress, July, 31th to August 3rd, 2012, Rio de Janeiro, RJ, Brazil.*

² *Physical, PhD., Federal University of São Carlos (UFSCar), São Carlos, SP, Brazil.*

³ *Physical,, PhD., Federal University of Maranhão (UFMA), São Luis, MA, Brazil.*

1 INTRODUCTION

Austenitic stainless steels have been used for more than half a century as orthopedic implant materials for fracture fixation and joint replacement. However, some aspect such as their low strength in the annealed conditions and their susceptibility to localized corrosion restrict the broader use of type of steel in orthopedic applications. Recent investigations have shown that a high nitrogen austenitic stainless steel, specified by the ISO 5823-9 standard as having a typical composition of 22Cr–10Ni–2.5Mo–0.4Nb–0.35N, combines high strength,⁽¹⁾ even in the annealed condition, and high localized corrosion resistance.⁽²⁾

Most orthopedic devices are manufactured by hot forging operations and require not only dimensional accuracy but also specific microstructural and mechanical properties. In these operations, power is generated by a source of energy, transmitted to the tools, which store the power elastically and transfer it to the workpiece through an interface. Consequently, the workpiece dissipates the power while undergoing plastic flow in the deformation zone. The material responds in two complementary ways: a rate of entropy production due to metallurgical changes and due to rising temperature (heat conduction). It has been proposed that power partitioning between these two ways is determined by the strain rate sensitivity of flow stress.^(3,4) The intrinsic workability, which is determined as the microstructure changes during deformation, depends on (i) the restoration processes such as dynamic recrystallization and dynamic recovery;⁽⁵⁻⁹⁾ (ii) damage process including cracks and fracture;⁽⁵⁻⁹⁾ and (iii) instability process such as flow localization and adiabatic shear band formation.⁽⁵⁻⁹⁾

During high temperature deformation, the internal structure evolves over time through hardening and softening mechanisms such work hardening, recovery and recrystallization, and the flow curve shapes depend on the competition between these phenomena. It has been established that, after certain amount of work hardening, materials having high level of stacking fault energy (SFE) soften by dynamic recovery, while materials with low SFE soften by dynamic recrystallization. When straining is applied at a constant temperature and strain rate, the flow rises in the initial work hardening regime and then becomes constant in high SFE materials. Conversely, the flow reaches a maximum before dropping to the steady state in low SFE materials. Austenitic stainless steels are normally considered as materials having low and intermediate SFE. For instance, the AISI 304L is about 18 mJ/m², while that of AISI 305 about 34 mJ/m², AISI 310S about 94 mJ/m², and AISI 316 about 78 mJ/m².⁽¹⁰⁾ The contribution of Ni, Cr, Mn and Mo to the SFE of an austenitic stainless steel matrix was estimated and the SFE calculated for ISO 5832-9 was found to be 68.7 mJ/m².⁽¹¹⁾ It has been observed that this intermediate level of SFE renders this material prone to cross slip and climb of dislocations, promoting high levels of static recovery. High levels of softening of as much as 60% can be promoted by recovery after hot deformation before and upon the onset of recrystallization. It has also been observed that, as the recrystallized fraction grows, the restoration promoted by recovery decreases over time but does not disappear.⁽¹¹⁾

The chemistry, microstructural complexity and use of the material make it imperative to understand the role of deformation parameters and to control of material's microstructural evolution during high temperature deformation. The objective of the present work was to analyze deformation behavior of the biomaterial under hot working conditions using different material models. The shape of experimental flow

stress curves was analyzed, a constitutive equation determined, processing maps were developed and microstructures observed.

2 MATERIAL AND METHODOS

The material used in this investigation was an ISO 5832-9 type stainless steel whose chemical composition is given in Table 1. It is worth noting the presence of niobium, chromium and nitrogen in this chemistry, which enable the formation of Z phase (NbCrN) under favorable conditions.

Table 1. Chemical composition of the ISO 5832-9 steel (mass %)

C	Si	Mn	Ni	Cr	Mo	S	P	N	Nb	Fe
0.035	0.37	4.04	10.6	20.3	2.47	0.001	0.022	0.36	0.29	bal.

Mechanical tests were carried out on a computerized hot torsion machine. Samples with a length and diameter of 10 mm in the reduced central gage section were heated in an induction furnace mounted directly on the testing machine. The temperature was measured using an optical pyrometer. Data were collected by means of a software program that imposes parametric tests such as temperature, strain rate, holding time and amount of straining. The samples were heated from room temperature to soaking temperature of 1,250°C, held at this temperature for 10 min, cooled to the test temperature at a rate of 2°C/s, held for 30 s, and finally strained isothermally to $\epsilon = 4.0$ or at sample fracture. These tests were carried out over temperature range of 900°C to 1,200°C and at equivalent strain rates of 0.01 s⁻¹, 0.5 s⁻¹, 1 s⁻¹ and 10 s⁻¹. To correlate the microstructure with the deformation conditions, the samples were immediately water-quenched after deformation. After standard metallographic procedures, the microstructure etched with nitric acidic (65%) was observed by optical microscopy (section longitudinal) and grain size was estimated in accordance with ASTM E112. The samples were cut along a plane parallel to the torsion axis, and then electropolished and etched by conventional.

3 RESULTS

3.1 Flow Stress Curves

Figure 1 depicts the plastic flow curves for stainless steel deformed in the range of 900°C to 1,200°C under strain rate of 0.01 s⁻¹ to 10 s⁻¹. In general, the flow stress rose in the initial work-hardening regime, reaching a maximum before dropping in the softening regime. The shape of the flow stress curve changed in both regions as the deformation conditions were altered; this variation was more noticeable in the softening regime. Three different types of flow stress curves that represent the dissipative nature were observed: (i) flow softening after a critical strain, leading to a steady state at higher strains (at higher temperatures and lower strain rates); (ii) continuous flow softening curves, as in Widmanstätten structures or in flow localization (at lower temperatures and higher strain rates); and (iii) a flat type, where the stress does not vary with strain, as observed in materials that recovery dynamically through the softening process (at lower temperatures and intermediate strain rates).

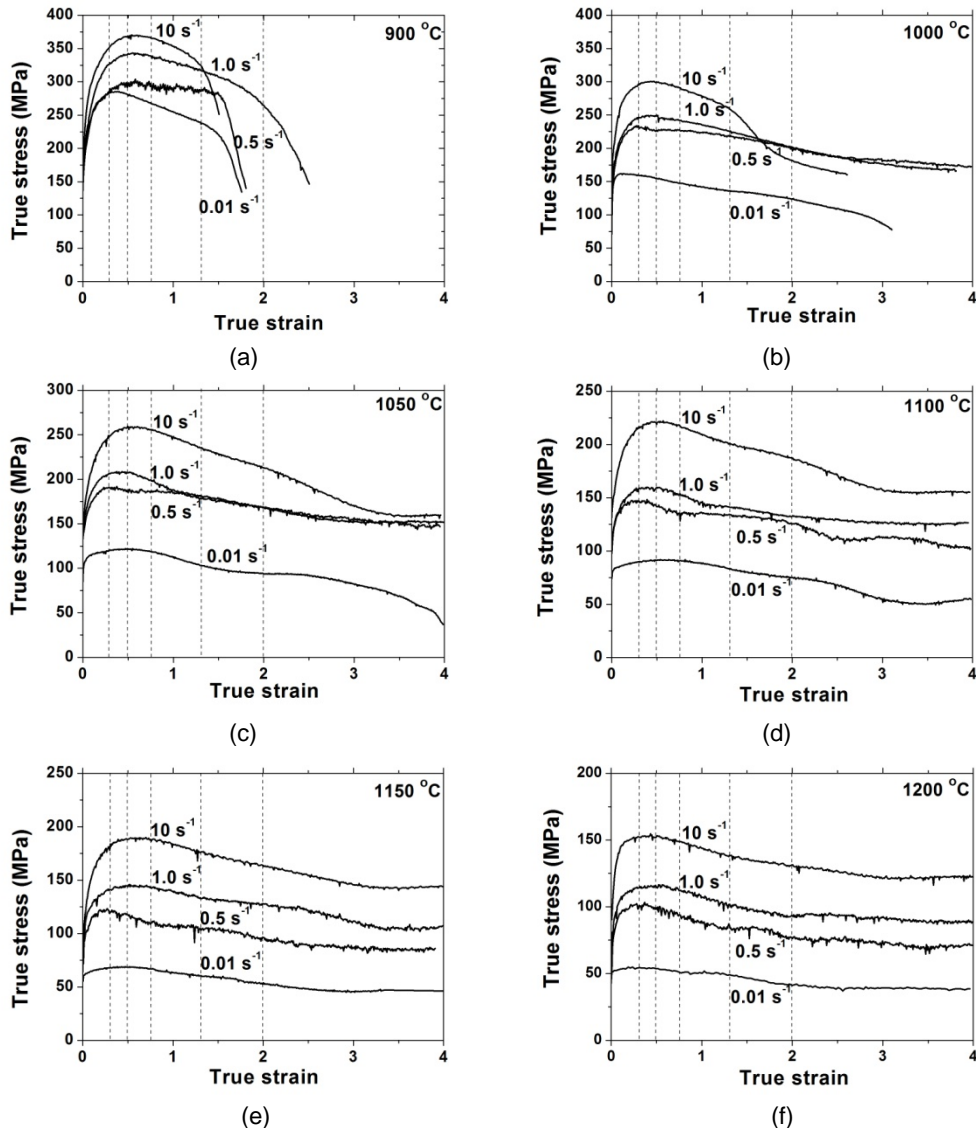


Figure 1. Flow curves attained for stainless steel studied at different strain rates and temperatures: (a) 900°C; (b) 1,000°C; (c) 1,050°C; (d) 1,100°C; (e) 1,150°C; and (f) 1,200°C.

As can be seen in Figure 1, at lower temperatures, the samples failed at lower strains than the one imposed in the experiments ($\epsilon = 4$). At 900°C, the samples broke down at a strain close to 2 under all the applied strain rates. Moreover, the test performed at 1,000°C with a strain rate of 10 s^{-1} failed under similar straining. In these experiments, it is worth noting that the drop in stress after the peak occurred continuously without reaching the steady state. Although the total strain was somewhat higher in the experiment conducted at 1000°C at a strain rate of 0.01 s^{-1} , the flow stress curve maintained the same decay rate as that exhibited in the above described experiments.

A steady-state stress was attained in all experiments conducted at higher temperatures. Although the shapes of the flow curves show some minor differences, these are characteristic of stress softening promoted by dynamic recrystallization. At high temperatures, the drop in stress between the peak stress and the steady state is relatively small, while the decay after the peak is sluggish and relatively higher at intermediate temperatures. Also, it can be noted that the yield stress is greater than steady state stress ($\sigma_0 > \sigma_{ss}$) in the experiments conducted at high temperatures with a strain rate of 0.01 s^{-1} .

3.2 Constitutive Equation

One of the initial attempts to evaluate the mechanism acting during plastic deformation was to determine a kinetic rate equation. Selecting the peak stress as the representative stress of each flow curve, the dependence of flow stress on strain rate and deformation temperature can be determined from Figure 1. In the range of deformation conditions employed here, this dependence can be described by the generalized hot-working relationship given by:

$$\dot{\epsilon} \exp(Q_{HW} / RT) = A [\sinh(\alpha \sigma_p)]^n = Z$$

Where A , α , n and Q_{HW} are material constants ($R=8.31$ J/mol.K). The Zener-Hollomon parameter (Z) encompasses the two control variables $\dot{\epsilon}$ and T . The kinetic rate equation for this steel can be written as:

$$\dot{\epsilon} = 1.492 \times 10^{19} [\sinh(0.011 \sigma_p)]^{4.5} \exp(-587000 / RT)$$

The Q_{HW} provides a simple description of the speed at which the flow stress rises or decreases in the hot working window. For instance, it shows how the flow stress rises as the temperature decreases from $0.8 T_m$ – at which alloys of the same metal are similar – to $0.5 T_m$ – at which more complex or concentrated alloys become much stronger or less ductile. Comparing this equation with stainless steels data in the literature, one finds that the n values are close and the activation energy of this steel is fairly high. An apparent activation energy of 500 kJ/mol was found for stainless steels with similar amounts of solid solution (~38%).⁽¹²⁾ It can therefore be speculated that the higher level of activation energy is associated with high nitrogen content and the presence of Z phase. The value of the stress exponent ($n = 4.5$) lies within the range of 3.6 to 5.0 which other authors have reported to correspond to dislocation climb.⁽¹³⁾

3.3 Development of Processing Maps

Another way to analyze plastic behavior under hot working conditions is by using a processing map. This map provides an explicit representation of the response of a material to the process parameters imposed upon it in terms of microstructural mechanisms, and consists of a superimposition of power dissipation and an instability map. Processing maps, which were developed based on the Dynamic Materials Model,^(3,4) consider the workpiece as a dissipater of power. The total dissipated power is related to the rate of entropy production. The entropy production due to metallurgical changes can be related to a dimensionless parameter called efficiency of power dissipation, η , given by:

$$\eta = 2m / (m + 1)$$

Where m is the strain rate sensitivity of the flow stress, which can be calculated using the following equation: $m = \Delta \ln \sigma / \Delta \ln \dot{\epsilon}$, with temperature and strain constants for a given history. Table 2 lists the calculated values as a function of the amount of strain and the deformation temperature of the steel under study. The variation de η with temperature and strain rate constitutes the power dissipation map (Figure 2), the domains of which may be interpreted in terms of a specific microstructural process.

Table 2. Dependency of strain rate sensitivity of flow stress with temperature and amount of deformation

Strain	Temperature (°C)					
	900	1,000	1,050	1,100	1,150	1,200
0.30	0.04	0.09	0.10	0.12	0.14	0.15
0.50	0.05	0.09	0.11	0.12	0.14	0.15
0.75	0.05	0.10	0.11	0.12	0.15	0.16
1.3	0.05	0.10	0.12	0.12	0.16	0.15
2.0	-	0.06	0.12	0.13	0.17	0.16

Table 2 indicates that the strain rate sensitivity of flow stress (m) increases with deformation temperature at the same strain and with the amount of straining at the same temperature. The variation in m lies within the range reported in the literature for stainless steels: 0.05 to 0.23.⁽¹⁴⁾ The calculated values at 900°C are two or three-fold lower than those determined at intermediate and high temperatures. These lower values are associated with the experiments in which the samples failed under low straining (Figure 1).

The stability criterion used in the Dynamic Materials Model considers the conditions for microstructural stability at a constant temperature in terms of a dimensionless parameter, (ξ), given by:

$$\xi(\dot{\epsilon}) = \frac{\partial \ln(m/(m+1))}{\partial \ln \dot{\epsilon}} + m > 0$$

The ξ parameter may be evaluated as a function of temperature and strain rate to obtain an instability map (Figure 2). This map may be superimposed on a power dissipation map to obtain a processing map.

Figure 2 displays processing maps developed for ISO 5832-9 austenitic stainless steel. In this figure, the variation in power dissipation efficiency with temperature and strain rate is represented as a contour map showing iso-efficiency contours in a temperature-strain rate plane. These maps were developed for different stages of flow stress curves: (i) in the work hardening regime with a strain of 0.3 (Figure 2a); (ii) around the peak stress with a strain of 0.5 (Figure 2b); and (iii) in the stress-softening regime with strain of 0.75, 1.3 and 2 (Figures 2c to 2e).

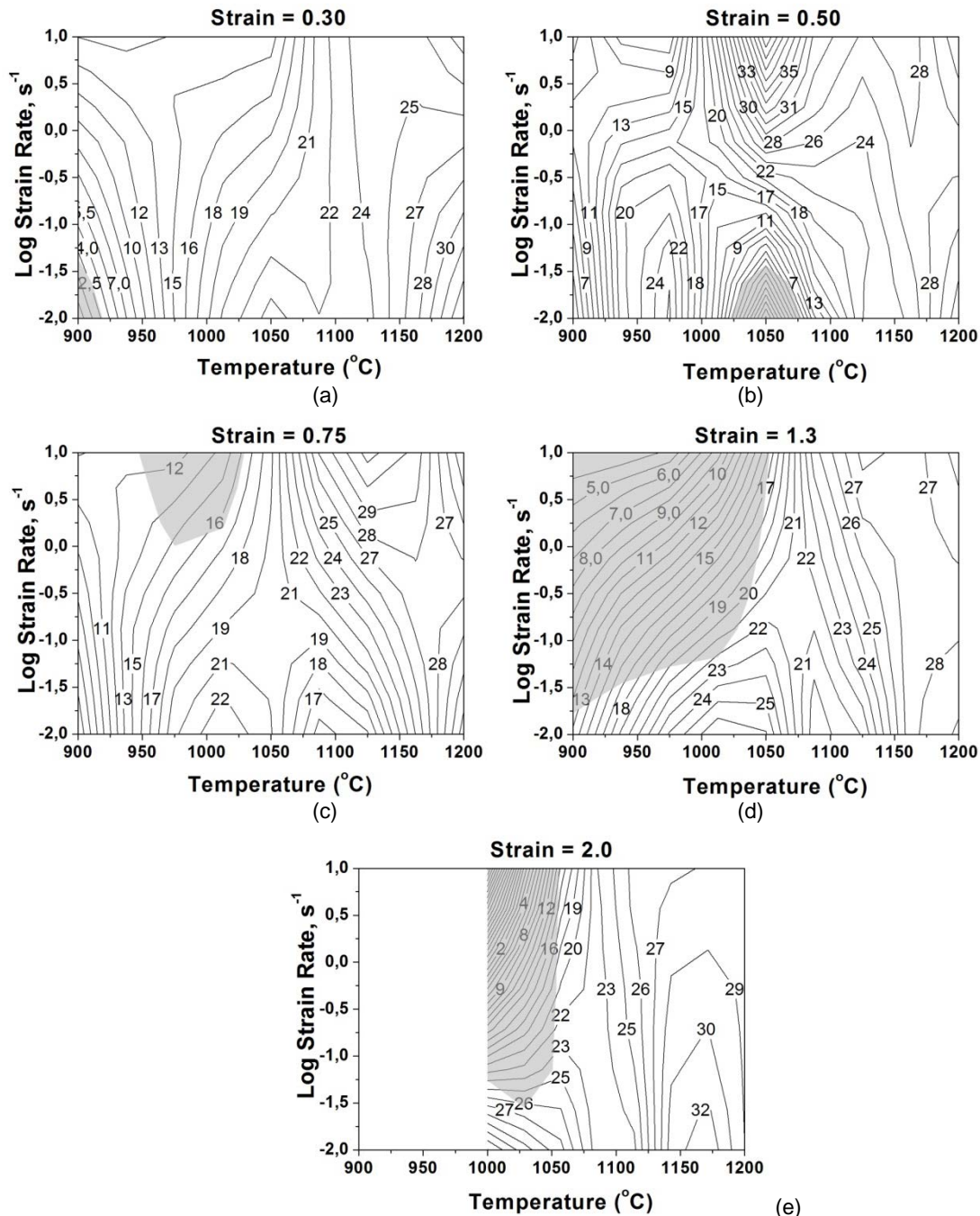


Figure 2. Processing maps for ISO 5832-9 steel at strains of (a) $\epsilon = 0.30$; (b) $\epsilon = 0.50$; (c) $\epsilon = 0.75$; (d) $\epsilon = 1.3$; and (e) $\epsilon = 2$.

In the stress-softening regime, the dissipation maps reveal two different safe domains: (i) in the range of 1,100°C to 1,200°C with an efficiency peak of 32% at 1,170°C and 0.01s⁻¹ with a strain of 2, and (ii) between 1,000°C to 1,170°C with an efficiency peak of 30% at 1,000°C and 0.01 s⁻¹ with a strain of 2. Processing maps also show an unstable domain at lower temperature and higher strain rates for strains that exceed the peak stress.

The safe domain at higher temperatures is revealed at low strains in the work hardening regime. However, the second safe domain revealed at lower temperatures and the unstable region observed at lower temperatures and higher strain rates are not indicated. With straining around the peak stress, the processing map indicated an

unstable region at low strain rates and a safe domain at a higher strain rate close to 1,050°C.

3.4 Microstructure Evolution

Since all samples were reheated at the same temperature before testing, they all showed the same initial material history. The starting microstructure is the one observed after reheating, a holding time of 600 s and water quenching. Figure 3 illustrates the starting microstructure, showing an austenitic matrix with equiaxed grains with an average size of 85 μm and numerous Z particles within and at the grain boundary. The second phase consists of different types of particles: (i) plate-like particles with sizes as large as 15 μm , (ii) round particles with size of 1 μm to 2 μm , and (iii) small particles with a size of about 0.3 μm .

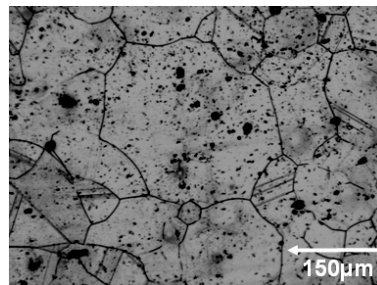


Figure 3. Austenite starting microstructure observed after reheating to 1,250°C, a holding time of 600 s and rapid cooling.

Some of the microstructures observed after straining and rapid cooling are depicted in Figures 4 to 6. Figure 4 shows microstructures of the samples that were deformed at higher temperatures in the high power dissipation domain. Here, tests were completed without sample failure; the amount of strain was 4. These micrographs reveal equiaxial grains whose average size depends on the conditions of deformation; an average size of 28.4 μm in Figure 4a, 26.6 μm in Figure 4b and 9.1 μm in Figure 4c. Bearing in mind that the average starting grain size was 85 μm , considerable grain refinement took place during deformation, allowing for the interference that dynamic recrystallization occurred.

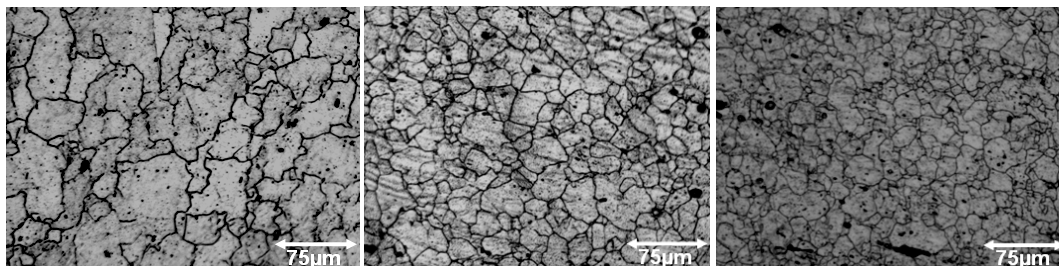


Figure 4. Microstructures observed after straining in the high power dissipation domain: (a) 1,200°C and 0.01 s^{-1} ; (b) 1,200°C and 10 s^{-1} ; and (c) 1,150°C and 1.0 s^{-1} .

Figure 5 displays microstructures observed after straining at intermediate temperatures. All the microstructures were recorded after straining to 4 and consist of numerous small recrystallized grains and old strained grains. Although the strain imposed belongs to steady state in the flow stress, it is clear that dynamic recrystallization was not complete. However, it is worth noting that the average recrystallized grain sizes are very small: 5 μm in Figure 5a and 4.9 μm in Figure 5b.

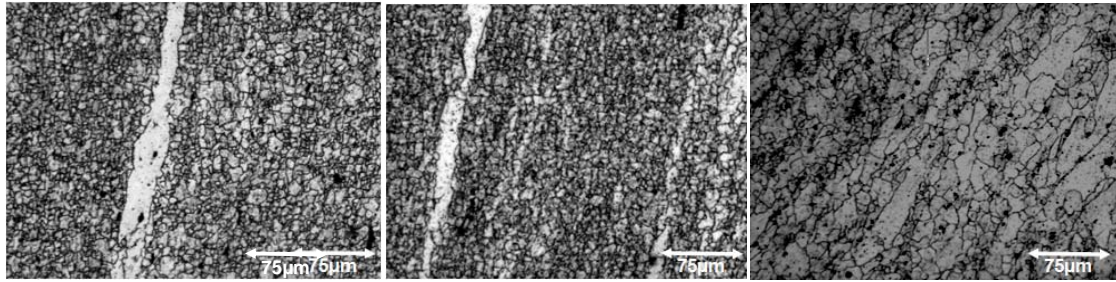


Figure 5. Microstructures recorded after straining at intermediate temperatures: (a) 1,100°C and 0.5 s⁻¹, (b) 1,050°C and 0.5 s⁻¹ and (c) 1,050°C and 10 s⁻¹.

In the region of plastic instability, samples fail after lower strains than that imposed in the experiments. Although the failure strains were higher than the peak strain, the microstructure displayed in Figure 6 indicates that the material was deformed essentially in the work hardening regime; straining old grains with a few small new grains at the grain boundaries. It is worth noting that samples that support large deformations before the onset of failure exhibited flow localization in the recrystallized region (Figures 6b and 6c).

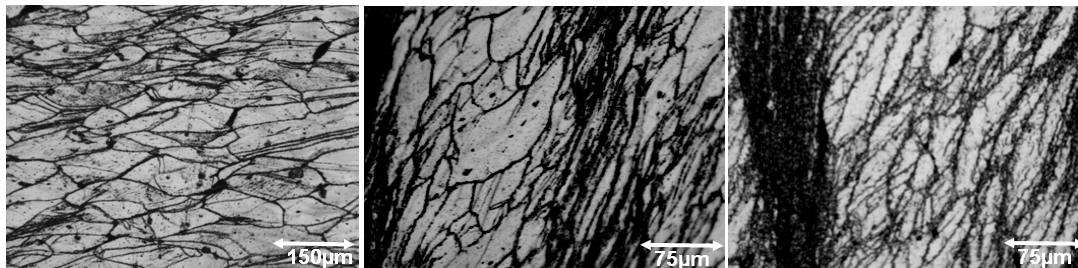


Figure 6. Microstructures recorded after straining in the region of plastic stability: (a) 900°C and 0.01 s⁻¹, (b) 1,000°C and 1.0 s⁻¹; and (c) 1,000°C and 0.01 s⁻¹.

4 DISCUSSION

Constitutive equations are normally used to calculate forces in processing at set rates. The value of activation energy determined here (587 kJ/mol) is an indication that the load must change significantly as the deformation temperature decreases and the strain rate increased. At high temperatures, the peak stress level of several stainless steels are similar, as described in McQueen and Ryan,⁽¹²⁾ but the difference becomes significant at low temperatures and high strain rates. A comparison of this steel with AISI 304 type ($Q_{HW} \sim 400$ kJ/mol) at 900°C and 10 s⁻¹ shows a difference is close to 80 MPa.⁽¹⁵⁾

The high strength of this steel suggests that work hardening is the dominant mechanism at lower temperatures and higher strain rates. In this region, the strain rate sensitivity of flow stress is low and processing maps display low levels of power dissipation. This represents a relatively low internal entropy production rate during hot deformation. In these conditions, the flow stress curves indicated that the material has low ductility and several experiments presented continuous flow softening curves after the peak stress without reaching the steady-state stress. The microstructure after continuous flow softening (Figures 6b and 6c) indicated that flow localization took place. In this case, the material system does not produce entropy constitutively at a rate that at least matches the rate of entropy input through imposed process parameters; the flow becomes localized and causes flow instability.

At straining close to peak stress, the instability map indicates an unstable regime close to 1,050°C and strain rate of 0.01s⁻¹. However, this unstable regime disappeared as the straining continued. In this deformation condition the flow stress curve shows an unusual behavior; the yield stress is higher than steady-state stresses ($\sigma_o > \sigma_{ss}$). Figure 7 depicts an enlarged part of the flow stress curve at 1,050°C and a strain rate of 0.01s⁻¹. Initially, the applied stress increases rapidly with the imposed deformation and, after a small deformation, the work hardening rate decreases continuously until the peak stress is reached. The change in the work hardening rate and the level of initial stress are evidence of the action of an additional hardening mechanism. In another research, fine Z phase precipitates were observed upon deformation under continuous cooling from a temperature below 1,100°C.⁽¹⁶⁾ During reheating at 1,250°C, dissolved particles may precipitate during cooling to deformation temperature or at the onset of straining. These fine precipitates are coherent with the matrix. Such coherence increases the degree of interaction between the precipitates and the glide dislocations, increasing the material's strength. As straining continues, the microstructure changes and the interfaces become incoherent.⁽¹⁷⁾

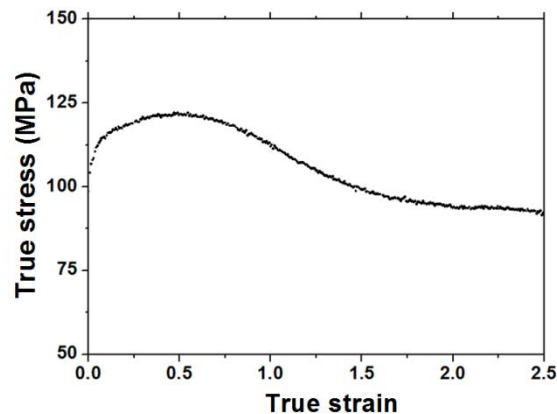


Figure 7. Experimental flow stress curve at 1,050°C and a strain rate of 0.01 s⁻¹.

Assuming that the difference in SFE estimated at room temperature is maintained at high temperature, some difference should be expected in the dynamic softening behavior of this biomaterial and other stainless steels with lower SFE. At lower temperatures some of the flow curves were flat: the stress did not vary with strain. The processing maps indicated low levels of power dissipation and the microstructures displayed pancake grains after straining beyond the peak stress. At intermediate temperatures, even after higher straining at steady-state stress, the microstructures contained recrystallized grains, although a significant volume fraction of deformed grains was still present. These features are strong evidence of extensive dynamic recovery and, as a consequence, dynamic recrystallization was delayed. Comparing these data with the behavior of AISI 304L which recrystallizes in the range of 1,000°C to 1,200°C at strain rates ranging from 5 s⁻¹ to 0.01 s⁻¹,⁽¹⁸⁾ it is clear that both steel have dynamic recrystallization features, but recrystallization is delayed in ISO 5832-9 and is only completed at higher temperatures.

One purpose of thermomechanical processing is to obtain a fine microstructure with equiaxial grains. Dynamic recrystallization is a mechanism that refines and favors the formation of this type of microstructure. However, due to competing hardening and softening mechanisms, a mixture of recrystallized and pancake grains may be present in partial recrystallized microstructures, as was in intermediate deformation

conditions. The final microstructure was composed of small grains, but the presence of pancake grains rendered it heterogeneous (Figure 4). This is a type of microstructure that should be avoided. Due to the broad range of deformation conditions in which partial recrystallization takes place, a combination of dynamic and static softening mechanisms is needed to produce a fine and uniform microstructure.

5 CONCLUSIONS

- Three different types of flow stress curves that represent the dissipative nature were observed: (i) flow softening after a critical strain, leading to a steady state at higher strain; (ii) continuous flow softening curves; and (iii) the flat type;
- the kinetic rate equation for this steel can be written as:

$$\dot{\epsilon} = 1.492 \times 10^{19} \left[\sinh(0.011 \sigma_p) \right]^{4.5} \exp(-587000/RT);$$

- the dissipation maps reveal two different safe domains: (i) in the range of 1,100°C to 1,200°C with a efficiency peak of 32% at 1,170°C and 0.01s⁻¹ with a strain of 2; and (ii) from 1,000°C to 1,170°C with an efficiency peak of 30% at 1,000°C and 0.01s⁻¹ with strain of 2. The processing maps also indicate an unstable domain at lower temperature and higher strain rates for strains exceeding the peak stress;
- at intermediate temperatures there was strong evidence of extensive dynamic recovery, thus delaying the dynamic recrystallization. As a consequence of the competition between hardening and softening mechanisms, a mixture of recrystallized and pancake grains may be present in partially recrystallized microstructures. This type of microstructure must be avoided.

Acknowledgements

The authors thank Capes (Brazil) for its financial support of this work.

REFERENCES

- 1 E.J. Giordani, V.A. Guimarães, T.B. Pinto, I. Ferreira, *Effect of precipitates on the corrosion-fatigue crack initiation of ISO 5832-9 Stainless Steel Biomaterials.* Inter. J. Fatigue 26 (2004) 1129-1136.
- 2 C. Ornhaugen, J.O. Nilsson, H. Vannevik, *Characterization of a nitrogen-rich austenitic stainless steel used for osteosynthesis devices.* J. Biomed. Mater. Research 31 (1996) 97-103.
- 3 Y.V.R.K. Prasad, T. Seshacharyulu, . *Optimization of cold and warm workability in 304 stainless steel using instability maps.* International Mater. Reviews, 43 (1998) 243–258.
- 4 Y.V.R.K. Prasad, S. Sasidhara, *Hot working guide: A compendium of processing maps*, OH: ASM International, Materials Park; Ohio, 1997.
- 5 S. Venugopal, S.L. Mannan, Y.V.R.K. Prasad, *Optimization of cold and warm workability in 304 stainless steel using instability maps.* J. Nuclear Mater. 227 (1995) 1-10.
- 6 Y.C. Lin, G. Liu, *Study of microstructural evolution during metadynamic recrystallization in a low-alloy steel.* Mater. Sci. Eng. A 523 (2009) 139-144.
- 7 S. Tan, Z. Wang, S. Cheng, Z. Liu, J. Han, W. Fu, *Processing maps and hot workability of Super304H austenitic heat-resistant stainless steel.* Mater. Sci. Eng. A 517 (2009) 312-315.
- 8 D. Cai, L. Xiong, W. Liu, G. Sun, M. Yao, *Development of processing maps for a Ni-based superalloy.* Mater. Characterization 58 (2007) 941-946.

- 9 F.L. Sui, L.X. Xu, L.Q. Chen, X.H. Liu, *Processing map for hot working of Inconel 718 alloy*. J. Mater. Process. Technol. 211 (2011) 433-440.
- 10 R.E. Schramm, R.P. Reed, *Stacking fault energies of seven commercial austenitic stainless steels*. Metall. Trans. A 6 (1975) 1345.
- 11 E.J. Giordani, A.M. Jorge Jr., O. Balancin, *Proportion of recovery and recrystallization during interpass times at high temperatures on a Nb- and N-bearing austenitic stainless steel biomaterial*. Scripta Mater. 55 (2006) 743-746.
- 12 H.J. McQueen, N.D. Ryan, *Constitutive analyze in hot working*. Mater. Sci. Eng. A 322 (2002) 43-63.
- 13 P. Adeva, G. Caruana, A.O. Ruano, M. Torralba, *Microstructure and high temperature mechanical properties of tin*. Mater. Sci. Eng. A 94 (1995) 17-23.
- 14 Z. Wenhui, S. Shuhua, Z. Deli Z, W. Baozhong, W. Zhenhua, F. Wantang, *Hot deformation behavior of a Nb- containing 316LN stainless steel*. Mater. Design 32 (2011) 4173-4179.
- 15 A.M. Jorge Jr., O. Balancin, *Prediction of Steel Flow Stresses under Hot Working Condition*. Mater. Research 8 (2005) 309-315.
- 16 E.J. Giordani, A.M. Jorge and O. Balancin, *Evidence of strain-induced precipitation on a Nb and N-Bearing austenitic stainless steel biomaterial*. Mater. Sci. Forum, 500–501 (2005), 179-186.
- 17 O. Balancin, W.A. Hoffmann, J.J. Jonas, *Influence of microstructure on the flow behavior of duplex stainless steels at high temperatures*. Metall. Mater. Trans. A 31 (2000) 1353-1364.
- 18 S. Venugopal, S.L. Mannan, Y.V.R.K. Prasad, *Optimization of cold and warm workability in 304 stainless steel using instability maps* Metall. Trans. A 23 (1992) 3093-3103.